# Optical Diffuse Imaging of an *Ex Vivo* Model Cancerous Human Breast Using Independent Component Analysis

Min Xu, Mohammad Alrubaiee, S. K. Gayen, and R. R. Alfano, *Fellow, IEEE*

***Abstract*—Optical imaging using independent component analysis (OPTICA) has been used for detection, 3-D localization, and cross-section imaging of a tumor inside a model human breast composed of *ex vivo* human breast tissues. OPTICA uses a multisource target illumination and multidetector signal acquisition scheme to obtain multiple spatial and angular views of the sample for target localization. Independent component analysis of the perturbations in the spatial light intensity distribution measured on the sample boundary sorts out the signal originating from individual targets. A back-projection technique estimates the cross-section of each target. The approach correctly provided the positions of a tumor located at the mid-plane and two glandular structures located at different positions within the 33-mm-thick model breast. The reconstructed cross-section images are in good agreement with known dimensions of the structures, and pathological findings.**

***Index Terms*—Breast cancer, diffuse optical imaging, independent component analysis, near infrared (NIR) imaging, optical mammography, optical imaging using independent component analysis (OPTICA).**

## I. Introduction

NEAR-INFRARED (NIR) diffuse optical tomography (DOT) is an emerging technology for functional characterization of biological tissues, and has been actively investigated to image lesions in human body organs, such as human breast [1]–[3], brain [4]–[7], and joints [8], [9]. A state-of-the-art DOT illuminates the sample (consisting of targets embedded in a turbid medium) with NIR light, measures the emergent light on the boundary of the turbid medium, and uses an iterative image reconstruction method for repeatedly solving the forward model of light propagation in the medium with an updated estimation of its optical properties to match the detected light intensities. This problem of imaging targets in a turbid medium is an ill-posed inverse problem, and *a priori* knowledge about the optical properties of the medium need to be used to obtain a unique solution at a cost of reduced resolution [10]–[13]. Various prior information such as anatomical structures obtained from X-ray or magnetic resonance imaging (MRI) and the absorption spectra of chromophores have been used to improve the imaging quality of the DOT [14]–[16]. The iterative image reconstruction is computation time intensive and reconstruction in 2-D planar sections instead of a 3-D volume is commonly practiced. Noniterative approaches have also been pursued [17]–[19]. Irrespective of these developments, reconstruction of images with adequate spatial resolution and accurate localization and characterization of the targets remain a formidable task.

We have developed an alternative approach for optical imaging using independent component analysis (OPTICA) [18], [20] that uses a multisource sample illumination and multidetector signal acquisition scheme to generate an extensive data set providing a variety of spatial and angular views of the medium. The signals from individual targets within the interrogated medium are then sorted out by using independent component analysis (ICA) based on their statistical independence. ICA is a statistical technique from information theory that is able to recover independent signals from their measured mixtures [21], [22]. ICA has been successfully applied in many biomedical applications, such as electroencephalogram (EEG) [23] and functional magnetic resonance imaging (fMRI) [24], and has been shown to be effective in separating signals from different brain activity centers. In DOT, excess light absorption or scattering by the individual targets embedded in the medium serve as the source of independent signals whose weighted mixture is recorded by a detector on the boundary of the medium. Since an independent component originating from any particular target relates directly to how light propagates from the source to the target and from the target to the detector, the recovered independent components can serve as the starting point for 3-D localization and optical characterization of individual targets in the medium. Such a staged procedure has been shown to significantly improve the sensitivity to small/weak absorptive, scattering and/or fluorescent targets, and can achieve a 3-D localization of the targets with remarkable accuracy and resolution [18], [25], [26].

The independent component is proportional to the strength of the target (the product of the difference in the absorption/scattering coefficient between the target and the background, and the volume of the target) and the convolution of the light propagators from the source to the target and from the

Manuscript received September 25, 2007; revised October 28, 2007. This work was supported in part by the U.S. Army Medical Research and Materials Command, in part by the Office of Naval Research (ONR), in part by the New York State Office of Science, Technology and Academic Research (NYSTAR), and in part by the City University of New York (CUNY) organized research programs. The work of M. Xu was supported by the Research Corporation and Fairfield University. The work of M. Alrubaiee was supported by the National Science Foundation (NSF) under Advance Placement Fellowship.

M. Xu is with the Department of Physics, Fairfield University, Connecticut, CT 06824 USA (e-mail: mxu@mail.fairfield.edu).

M. Alrubaiee is with the Department of Physics, City College and the Graduate Center, City University of New York, New York, NY 10031 USA (e-mail: malrub@sci.ccny.cuny.edu).

S. K. Gayen and R. R. Alfano are with the Institute for Ultrafast Spectroscopy and Lasers, City College and the Graduate Center, City University of New York, New York, NY 10031 USA (e-mail: gayan@sci.ccny.cuny.edu; ralfano@sci.ccny.cuny.edu).

Color versions of one or more of the figures in this paper are available online at http://ieeexplore.ieee.org.

Digital Object Identifier 10.1109/JSTQE.2007.912831

target to the detector. The two light propagators can be deconvoluted in the Fourier space. A 2-D cross-section image of the target is obtained by back projecting the independent component onto the transversal plane at the axial location of the target. Every independent component retrieved by ICA represents the signal from only one target with localization determined from earlier stage of analysis. So, a back projection formalism with little or no regularization can be applied to obtain a cross-section image of the target with improved spatial resolution than what is feasible in a conventional DOT.

We have previously tested the efficacy of OPTICA on samples consisting of absorbing or scattering targets within tissue phantoms and fluorescent targets in *ex vivo* tissue [18], [25], [26]. In this paper, we use OPTICA to investigate a tumor and other structures embedded in a "realistic" model breast assembled using *ex vivo* human breast tissues, as a prelude to *in vivo* breast imaging. The remainder of the paper is organized as follows. Section II presents the theoretical formalism of OPTICA and the back-projection approach for obtaining the cross-section image of a target. Section III describes the experimental arrangement, method, and parameters. Experimental results appear in Section IV. The implications are discussed in Section V.

## II. Theoretical Formalism of Optical Imaging Using Independent Component Analysis

The presence of targets (optical inhomogeneities) inside a turbid medium perturbs the spatial intensity distribution of light emergent from the medium under illumination by a probing beam. When illuminated by a point source of unit power, the change in the light intensity distribution on the boundary of the specimen due to absorptive and scattering targets can be written as [27], [28]

$$-\Delta I(\mathbf{r}_d,\mathbf{r}_s)=\int d^3\mathbf{r}\,\delta\mu_a(\mathbf{r})\,cG(\mathbf{r}_d,\mathbf{r})\,G(\mathbf{r},\mathbf{r}_s)+\int d^3\mathbf{r}\,\delta D(\mathbf{r})\,c\nabla_{\mathbf{r}}\,G(\mathbf{r}_d,\mathbf{r})\nabla_{\mathbf{r}}G(\mathbf{r},\mathbf{r}_s)\quad(1)$$

in the first-order Born approximation assuming that light diffuses inside the medium [29]. Here, $\mathbf{r}_s$ and $\mathbf{r}_d$ are the positions of the source and the detector on the boundary, $\delta\mu_a(\mathbf{r})=\mu_a(\mathbf{r})-\mu_{a_0}$ and $\delta D(\mathbf{r})=D(\mathbf{r})-D_0$ are the differences in absorption coefficient and diffusion coefficient, respectively, between the target at $\mathbf{r}$ and the background medium, $c$ is the speed of light in the medium, and $G(\mathbf{r},\mathbf{r}')$ is the Green's function describing light propagation from $\mathbf{r}'$ to $\mathbf{r}$ inside the medium of absorption coefficient $\mu_{a_0}$ and diffusion coefficient $D_0$.

OPTICA assumes each inhomogeneity within the turbid medium to be a virtual source and expresses the change of the light intensity on the boundary of the specimen as

$$-\Delta I(\mathbf{r}_d,\mathbf{r}_s)=\sum_j a_j(\mathbf{r}_d)\,s_j(\mathbf{r}_s)\quad(2)$$

where $s_j(\mathbf{r}_s)$ represents the $j$th target illuminated by the incident wave at $\mathbf{r}_s$ and $a_j(\mathbf{r}_d)$ is the weighting matrix describing the propagation of light from the $j$th inhomogeneity to the detector at $\mathbf{r}_d$. Each absorptive inhomogeneity contributes one term in (2), and each scattering inhomogeneity contributes three terms in (2) [18]. The detected change of the light intensity $-\Delta I$ is, hence, a linear mixture of signals where $a_j$ and $s_j$ can now be interpreted as the *j*th weighting matrix and virtual source, respectively. Owing to the statistical independence between these virtual sources, independent component analysis of $-\Delta I$ will yield a list of independent components and recover both $a_j$ and $s_j$. Here, $a_j$ and $s_j$ are the independent intensity distribution on the detector and source planes, respectively, for the $j$th target. The number of the leading independent components gives the number of objects. The location of the *j*th target is obtained from the analysis of the retrieved independent component ($s_j$ and $a_j$) that relates directly to the source-to-object and object-to-detector Green's functions $G(\mathbf{r}_j,\mathbf{r}_s)$ and $G(\mathbf{r}_d,\mathbf{r}_j)$ and the optical property of the target where $\mathbf{r}_j$ is the position of the $j$th object [18], [20], [25], [26].

For the slab geometry investigated here, there are three virtual sources of specific patterns (one centrosymmetric and two dumbbell-shaped) associated with each scattering inhomogeneity, whereas only one centrosymmetric virtual source is associated with each absorptive inhomogeneity. Among the three virtual sources associated with a scattering inhomogeneity, the centrosymmetric virtual source is the strongest and more amenable to detection in a thick turbid medium [25]. The centrosymmetric virtual source and the corresponding weighting matrix are $s_j\propto G(\mathbf{r}_j,\mathbf{r}_s)$ and $a_j\propto G(\mathbf{r}_d,\mathbf{r}_j)$, and $s_j\propto\partial G/\partial z(\mathbf{r}_j,\mathbf{r}_s)$ and $a_j\propto\partial G/\partial z(\mathbf{r}_d,\mathbf{r}_j)$, respectively, for absorptive and scattering inhomogeneities. A simple least square fitting of the centrosymmetric component, such as

$$\min_{\mathbf{r}_j,\alpha_j,\beta_j}\left\{\sum_{\mathbf{r}_s}\left[\alpha_j^{-1}s_j(\mathbf{r}_s)-G(\mathbf{r}_j,\mathbf{r}_s)\right]^2+\sum_{\mathbf{r}_d}\left[\beta_j^{-1}a_j(\mathbf{r}_d)-G(\mathbf{r}_d,\mathbf{r}_j)\right]^2\right\}\quad(3)$$

for the absorptive object, can be used to yield the 3-D location $\mathbf{r}_j$ and the strength $\alpha_j\beta_j$ of the target. When *a priori* knowledge about the property of the target is not available, (3) can still be used to estimate the 3-D location of the target regardless of the absorption or scattering property of the target. This is due to the fact that $\partial G/\partial z(\mathbf{r}_j,\mathbf{r}_s)\simeq-\kappa G(\mathbf{r}_j,\mathbf{r}_s)$ and $\partial G/\partial z(\mathbf{r}_d,\mathbf{r}_j)\simeq-\kappa G(\mathbf{r}_d,\mathbf{r}_j)$, where $\kappa=\sqrt{(\mu_{a_0}-i\omega/c)/D_0}$ is chosen to have a nonnegative real part with $\omega$ the modulation frequency of the incident wave.

The signal from the *j*th target is simply given by $-\Delta I_j=a_j(\mathbf{r}_d)s_j(\mathbf{r}_s)$. On the other hand, the centrosymmetric signal of the *j*th target can be approximated as a double convolution

$$-\Delta I_j(\mathbf{r}_d,\mathbf{r}_s)=\int G(\boldsymbol{\rho}_d-\boldsymbol{\rho},z_d,z_j)\,X_j(\boldsymbol{\rho})\,G(\boldsymbol{\rho}-\boldsymbol{\rho}_s,z_j,z_s)d\boldsymbol{\rho}\quad(4)$$

where the integration is over the $z=z_j$ plane, $X_j$ represents the target, and $\boldsymbol{\rho}_d$ and $\boldsymbol{\rho}_s$ are the lateral coordinates of the detector and the source, respectively. The cross-section image of the *j*th target $X_j$ is a 2-D distribution of the absorption/scattering coefficient of the target on the $z=z_j$ plane. In the Fourier space,

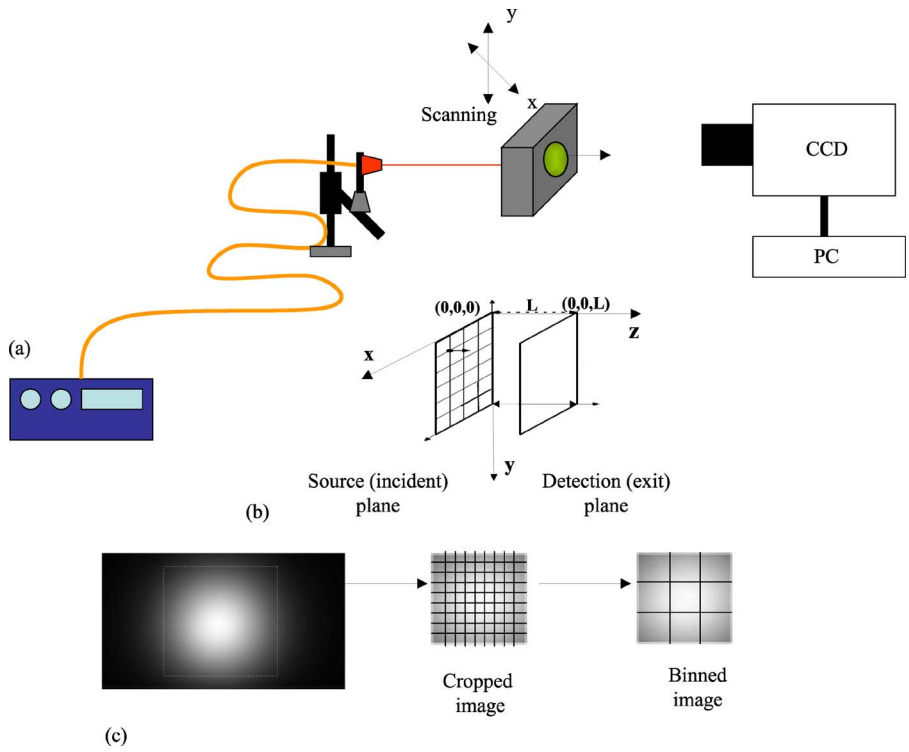


Fig. 1. (a) Schematic diagram of the experimental arrangement. CCD, charge coupled device; PC, personal computer. (b) Expanded view of the sample input (source) plane and exit (detection) plane showing the grid points in the $x$–$y$ plane. (c) Typical raw CCD image of the detection plane, and how it is cropped and binned for analysis.

the target function $X_j$ can be obtained from (4) as

$$X_j(\mathbf{q}) = -\frac{\Delta I_j(\mathbf{q}-\mathbf{q}_s, \mathbf{q}_s)}{G(\mathbf{q}-\mathbf{q}_s, z_d, z_j)G^*(\mathbf{q}_s, z_j, z_s)} \tag{5}$$

where $\mathbf{q}$ and $\mathbf{q}_s$ are the spatial frequency on the lateral plane and "$*$" denotes complex conjugate. We choose $\mathbf{q}_s = 0$ in the evaluation of the target function (5) since sources are usually much sparser than detectors in our setup where a charge-coupled device (CCD) camera is used to detect the emergent light intensity on the surface of the medium. The inverse Fourier transforms of $X_j(\mathbf{q})$ yields the high-resolution cross-section image of the $j$th target due to the high density of detecting pixels of the CCD. The size of the target is estimated by the full-width at half-maximum (FWHM) of the cross-section image $X_j$.

To sum up, OPTICA first detects and retrieves independent components corresponding to each target embedded inside a turbid medium, then obtains the 3-D location and strength of the target from these independent components, further reconstructs the cross-section image of the target on the transversal plane where the target locates, and finally, the size and the optical property of the target are estimated.

## III. Experiment

The experimental arrangement for detection and localization of the tumor in the *ex vivo* model breast sample is shown in Fig. 1(a). The model breast was a 70 mm × 55 mm × 33 mm slab composed of excised female human breast tissues provided to us by National Disease Research Interchange under an Internal Review Board approval at the City College of New York. The model breast was assembled using two pieces of *ex vivo* human breast tissues. The larger piece was normal tissue that included mainly adipose tissue and streaks of fibroglandular tissues. The existence of the fibroglandular tissues was not known prior to making the measurements.

The second piece was mainly a tumor (infiltrating ductal carcinoma) with a small amount of normal tissues in the margins with an overall approximate dimension of 8 mm × 5 mm × 3 mm. An incision was made in the mid-plane (along the $z$-axis, which was the shorter dimension of the tissue) of the normal piece, and some amount of the normal tissue was removed from the central region making a small pouch. The tumor piece was then inserted into the pouch, and the incision was closed by moderate compression of the composite consisting of the normal tissue and the tumor along $xyz$-directions. The breast tissue slab was contained inside a transparent plastic box. One of the sides of the box could be moved to uniformly compress the tissue along the $z$-axis and hold it in position. The resulting specimen, a 70 mm × 55 mm × 33 mm slab, was treated as one entity in the subsequent imaging experiment. The position of the tumor within the slab was known since it was placed in the position as discussed earlier. One of the tests of the efficacy of this imaging approach was to see how well the known position is assessed.

A 200 $\mu$m optical fiber delivered a 784 nm, 300 mW continuous-wave beam from a diode laser for sample illumination. The beam was collimated to a 1 mm spot onto the entrance face (henceforth referred to as the "source plane")

of the slab sample. Multiple source illumination was realized in practice by step scanning the slab sample across the laser beam in an $xy$ array of grid points using a computer-controlled translation stage. The $xy$ array was $22 \times 16$ with a step size of 2.0 mm. The signal from the opposite face of the sample (henceforth referred to as the "detection plane") was collected by a camera lens and projected onto the sensing element of a cooled 16 b, $1024 \times 1024$ pixel CCD camera. Although the scanned area is 42 mm $\times$ 30 mm on the source plane, the imaged area of the detection plane was much larger, covering the entire 70 mm $\times$ 55 mm transverse area of the model breast. Each illuminated pixel of the CCD camera could be regarded as a detector. For illumination of every scanned point on the source plane, the CCD camera recorded the diffusely transmitted 2-D intensity pattern on the detection plane. Each image acquisition took 100 ms, and one stepping of the translational stage took 1 s. A total of 352 images were completed within 7 min. The OPTICA reconstruction and cross-section imaging is expected to be completed within 2 min once fully automated.

## IV. Results

A typical 2-D raw image of transmitted light intensity distribution on the detector plane for illumination at a typical scanning position is shown in Fig. 1(c). The average of all the $22 \times 16$ images was used to obtain the optical property of the slab of breast tissue. The radial profile of the intensity of the transmitted light on the average image was fitted to that predicted by a diffusion model of light propagation inside a slab. The transport mean free path was assumed to be 1 mm, the value for a typical human breast tissue at 785 nm. The reduced scattering coefficient was then 1 mm$^{-1}$. From the decay of the radial profile of the intensity of the transmitted light, the average absorption coefficient of the entire model breast is found to be $\mu_a = 0.0039$ mm$^{-1}$. Each raw image is first cropped to retain the region within the window of 50.4 mm $\times$ 51.3 mm (out of a total 70 mm $\times$ 55 mm transverse area of the model breast) over which image reconstruction would be performed. The size of 1 pixel in the raw image is 187 $\mu$m $\times$ 187 $\mu$m. The raw images are binned by merging $5 \times 5$ pixels into one to enhance the SNR, resulting in a total of 352 images of $54 \times 55$ pixels each. All the binned images corresponding to illumination of the grid points in sequence were then stacked, and used as input for independent component analysis.

The independent light intensity distributions obtained by OPTICA is displayed in Fig. 2(a). The 3-D location of the targets were obtained from least squares fitting using (3). The fittings of the independent light intensities over lines passing through the maximum value and along the horizontal direction are displayed in Fig. 2(b). The tumor C is found at 14.8 mm from the detection plane and centered at (33.3, 21.5, 18.2) mm. In addition, two glandular sites were identified. The first glandular site A is found to be located at 2.5 mm from the detection plane and centered at (11.2, 22.4, 30.5) mm; the second glandular site B is at 14.6 mm from the detection plane and centered at (21.5, 37.3, 18.4) mm. Comparison of known and 3-D positions obtained from OPTICA for the cancer site and two glandular sites is given in Table I.

The cross-section image of the tumor obtained from a 2-D inverse Fourier transform of (5) is shown in Fig. 3 (left pane). The right pane of Fig. 3 displays the intensity profiles of the cross-section image along the $x$- and $y$-directions denoted by the white dashed lines. The FWHM values of the intensity profiles yield estimates of the lateral dimensions of the tumor to be 10.3 mm $\times$ 7.4 mm, while the known dimensions are 8 mm $\times$ 5 mm. Histological micrograph of the suspect site confirmed tumor. Similar back-projection cross-sectional images and histological micrographs were obtained (not shown here) for the glandular tissues as well and their transverse sizes were estimated from OPTICA. The existence, location, and size of the glandular tissues were not known *a priori*. The glandular structure A near surface is estimated to be 2.7 and 1.6 mm in size along the $x$- and $y$-directions from the cross-section image, respectively. The size of the glandular structure B at the midplane is 8.7 and 9.2 mm in size along the $x$- and $y$-directions, respectively.

Low regularization was used in generating the cross-section images in Fig. 3 to achieve maximal spatial resolution. The artifacts in the cross-section images can be suppressed with a higher regularization at a cost of lower spatial resolution. Since the target has been localized in the earlier stage of analysis, the target will not be confused with artifacts in the cross-section images and low regularization is beneficial here.

The investigated *ex vivo* breast sample contained minimal amount of blood, and hence, the reconstructed images are for the scattering property of the sample. The change of the reduced scattering coefficient $\mu_s'$ for the targets can further be estimated from the reconstructed independent components for the sites A, B and C. The value of $\delta\mu_s'$ is given by the ratio of the strength of the target and its volume. The sites A and B have lower scattering while the site C has enhanced scattering compared to the background (mainly adipose tissue). The values of $\delta\mu_s'$ are $\sim$0.2 and $\sim -0.4$ mm$^{-1}$ for the tumor and glandular tissues, respectively. Subsequent pathological analysis confirmed the site C as infiltrating ductal carcinoma, and identified the other two structures as glandular breast tissues.

## V. Discussion

The results of the experiments clearly demonstrate that OPTICA can locate the tumor inside the model breast with high accuracy. As can be seen from Table I, the lateral positions of the tumor agree within 0.5 mm, while the axial position agree within $\sim$1 mm of the known values. Similar high accuracy in the respective positions of the two pieces of glandular tissues is observed as well. The accuracy of the lateral positions does not depend significantly on the depth of the targets, while that of the axial position shows a weak dependence. For the target located close to the detection plane (glandular site A at a distance of 2.5 mm from the detection plane), the axial position is determined exactly, while for targets in the midplane that are much more challenging to locate, the accuracy is within 1 mm. Given

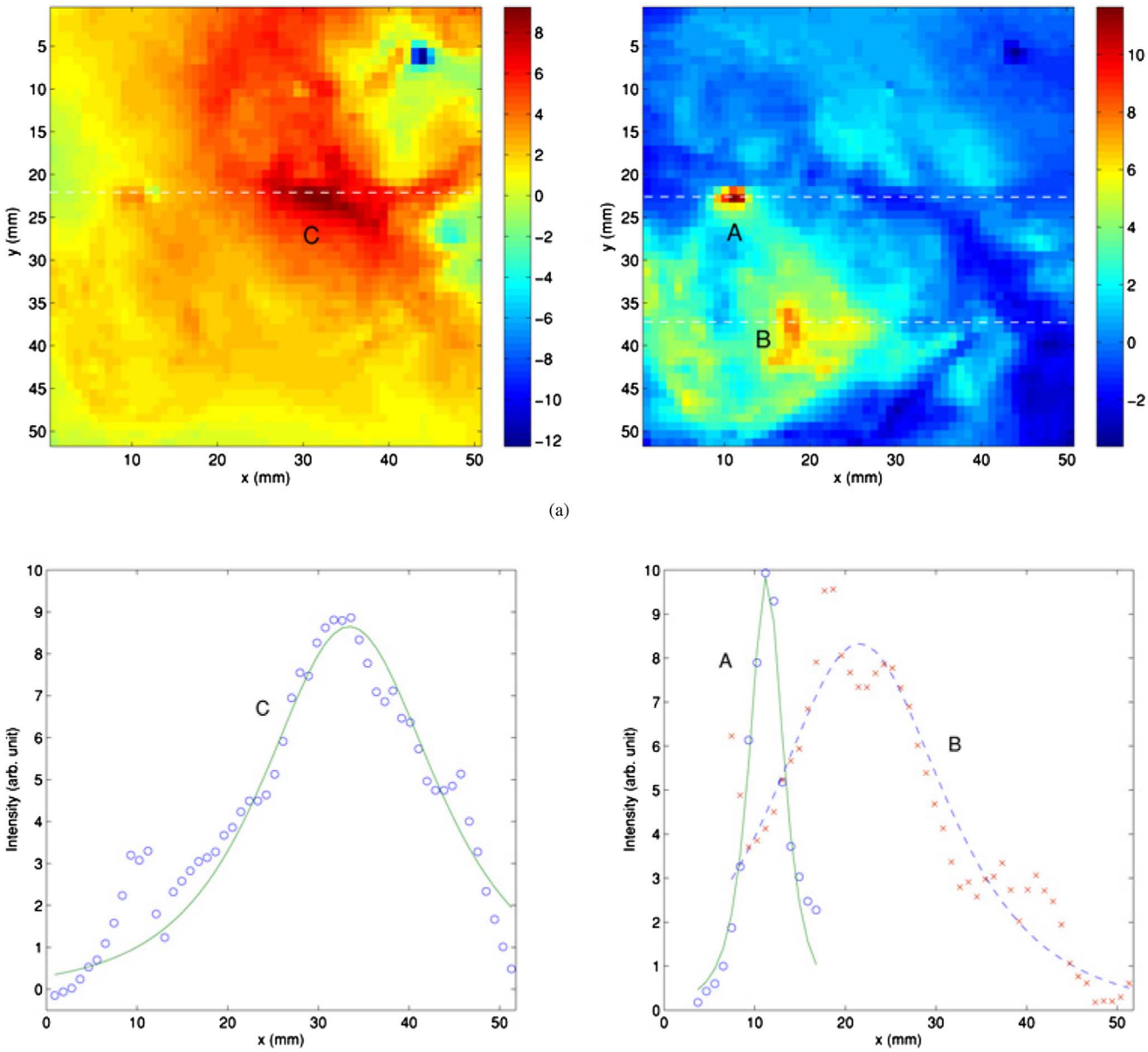


Fig. 2. (a) Independent intensity distribution on the detector plane ($z = 33$ mm) obtained by OPTICA for the tumor C (left pane) and the glandular structures A and B (right pane). (b) Corresponding bottom panes show the Green's function fits (solid lines) to the horizontal spatial profile (denoted by circles and crosses) through the center of the intensity distributions along the dashed lines.

TABLE I
COMPARISON OF KNOWN AND OPTICA ESTIMATED TARGET LOCATIONS

| Target | Known Position $(x, y, z)$ (mm) | OPTICA Estimated Position $(x, y, z)$ (mm) |
|---|---|---|
| Cancer Site (C) | (33,21,16.9) | (33.3,21.5,18.2) |
| Glandular Site (A) | (11,22,30.5) | (11.2,22.4,30.5) |
| Glandular Site (B) | (21,37,17) | (21.5,37.3,18.4) |

that light propagation is highly diffusive in breast tissues, this level of accuracy is quite significant.

The back-projection formalism estimates the FWHM values of the lateral dimension of the tumor to be 10.3 and 7.4 mm in size along the $x$- and $y$-directions, respectively, whereas the known dimension is 8 mm $\times$ 5 mm. This result is expected due to diffusion of light in the tissue, and is in line with the results that we obtained in our earlier OPTICA studies [26].

Another important finding was that OPTICA predicted different scattering properties for the adipose tissue (medium), the tumor, and the glandular tissues. The glandular tissues were found to be less scattering than the adipose tissues at the wavelength of interrogation, i.e., 784 nm. The tumor was found to be more scattering. These observations are consistent with the known literature values of scattering properties of different types of tissues [30].

The nature of the inhomogeneity (either absorptive or scattering or mixed) can be discerned by OPTICA with continuous-wave measurement when the SNR is high [20], [25]. When the SNR is not favorable, the recovered independent component

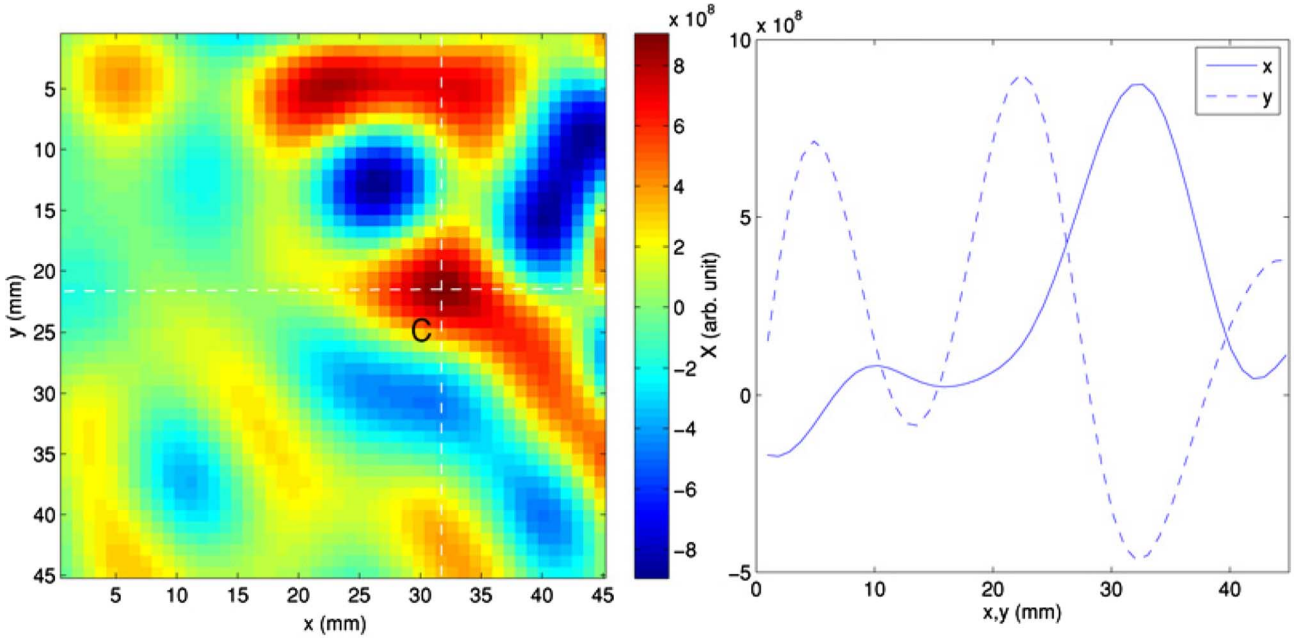


Fig. 3. Cross-section image of the tumor at the $z = 18.2$ mm plane formed by back-projection (left pane). Right pane: Spatial profiles of the cross-section image along the $x$- and $y$-directions shown by the white dashed lines (right pane). The FWHM of the cancer site is 10.3 and 7.4 mm along the $x$- and $y$-directions, respectively.

will be due to both absorption and scattering perturbations at the site of the inhomogeneity. The strength of the target will be proportional to $\delta\mu_a + \kappa^2\delta D = \delta\mu_a + (\mu_{a_0} - i\omega/c)\delta D/D_0$, which provides a way to discriminate between absorption and scattering if measurements of multiple modulation frequencies $\omega$ are available. The capability of OPTICA for separating absorption from scattering inhomogeneities can be significantly improved with a time-domain or frequency-domain measurement. Another enabling factor will be carrying out multispectral OPTICA studies for potential diagnostic information.

OPTICA can be used for fluorescent targets as well [26]. The same experimental arrangement may be used, except for the introduction of filters to block the excitation beam and to transmit the fluorescence light. What is even more interesting is that, a beam-splitter and two detectors combination with appropriate filters may be used to simultaneously pursue absorption/scattering OPTICA and fluorescence OPTICA studies of biological samples for obtaining coregistered information from dual probes.

OPTICA is suited to detect small objects. Given its ability to identify low-contrast small objects, the approach is expected to be especially useful for the detection of breast and prostate tumors at their early stages of growth.

## ACKNOWLEDGMENT

The authors acknowledge Dr. W. Cai for his helpful discussions.

## REFERENCES

[1] B. Chance, S. Nioka, J. Zhang, E. F. Conant, E. Hwang, S. Briest, S. G. Orel, M. D. Schnall, and B. J. Czerniecki, "Breast cancer detection based on incremental biochemical and physiological properties of breast cancers: A six-year, two-site study," *Acad. Radiol.*, vol. 12, pp. 925–933, Aug. 2005.

[2] R. Choe, A. Corlu, K. Lee, T. Durduran, S. D. Konecky, M. Grosicka-Koptyra, S. R. Arridge, B. J. Czerniecki, D. L. Fraker, A. DeMichele, B. Chance, M. A. Rosen, and A. G. Yodh, "Diffuse optical tomography of breast cancer during neoadjuvant chemotherapy: A case study with comparison to MRI," *Med. Phys.*, vol. 32, pp. 1128–1139, Apr. 2005.

[3] B. Brooksby, B. W. Pogue, S. Jiang, H. Dehghani, S. Srinivasan, C. Kogel, T. D. Tosteson, J. Weaver, S. P. Poplack, and K. D. Paulsen, "Imaging breast adipose and fibroglandular tissue molecular signatures by using hybrid MRI-guided near-infrared spectral tomography.," *Proc. Natl. Acad. Sci. USA*, vol. 103, pp. 8828–8833, Jun. 2006.

[4] J. C. Hebden, A. Gibson, T. Austin, R. M. Yusof, N. Everdell, D. T. Delpy, S. R. Arridge, J. H. Meek, and J. S. Wyatt, "Imaging changes in blood volume and oxygenation in the newborn infant brain using three-dimensional optical tomography," *Phys. Med. Biol.*, vol. 49, pp. 1117–1130, Apr. 2004.

[5] T. Durduran, G. Yu, M. G. Burnett, J. A. Detre, J. H. Greenberg, J. Wang, C. Zhou, and A. G. Yodh, "Diffuse optical measurement of blood flow, blood oxygenation, and metabolism in a human brain during sensorimotor cortex activation," *Opt. Lett.*, vol. 29, pp. 1766–1768, Aug. 2004.

[6] M. A. Franceschini, D. K. Joseph, T. J. Huppert, S. G. Diamond, and D. A. Boas, "Diffuse optical imaging of the whole head," *J. Biomed. Opt.*, vol. 11, no. 5, pp. 054007-1–054007-10, 2006.

[7] A. P. Gibson, T. Austin, N. L. Everdell, M. Schweiger, S. R. Arridge, J. H. Meek, J. S. Wyatt, D. T. Delpy, and J. C. Hebden, "Three-dimensional whole-head optical tomography of passive motor evoked responses in the neonate.," *Neuroimage*, vol. 30, pp. 521–528, Apr. 2006.

[8] Y. Xu, N. Iftimia, H. Jiang, L. L. Key, and M. B. Bolster, "Three-dimensional diffuse optical tomography of bones and joints," *J. Biomed. Opt.*, vol. 7, pp. 88–92, 2002.

[9] A. H. Hielscher, "Optical tomographic imaging of small animals," *Curr. Opin. Biotechnol.*, vol. 16, pp. 79–88, Feb. 2005.

[10] A. N. Tikhonov and A. V. Goncharsky Eds., *Ill-Posed Problems in the Natural Sciences*. Moscow, Russia: MIR, 1987.

[11] S. R. Arridge, "Optical tomography in medical imaging," *Inverse Prob.*, vol. 15, pp. R41–R93, 1999.

[12] X. Intes and B. Chance, "Non-pet functional imaging techniques: Optical," *Radiol. Clin. North Amer.*, vol. 43, no. 1, pp. 221–234, Jan. 2005.

[13] A. P. Gibson, J. C. Hebden, and S. R. Arridge, "Recent advances in diffuse optical imaging," *Phys. Med. Biol.*, vol. 50, pp. R1–R43, Feb. 2005.

[14] V. Ntziachristos, A. G. Yodh, M. D. Schnall, and B. Chance, "MRI-guided diffuse optical spectroscopy of malignant and benign breast lesions," *Neoplasia*, vol. 4, no. 4, pp. 347–354, 2002.
[15] A. Corlu, T. Durduran, R. Choe, M. Schweiger, E. M. C. Hillman, S. R. Arridge, and A. G. Yodh, "Uniqueness and wavelength optimization in continuous-wave multispectral diffuse optical tomography," *Opt. Lett.*, vol. 28, pp. 2339–2341, Dec. 2003.
[16] S. Srinivasan, B. W. Pogue, B. Brooksby, S. Jiang, H. Dehghani, C. Kogel, W. A. Wells, S. P. Poplack, and K. D. Paulsen, "Near-infrared characterization of breast tumors in vivo using spectrally-constrained reconstruction," *Technol. Cancer Res. Treat.*, vol. 4, pp. 513–526, Oct. 2005.
[17] W. Cai, S. K. Gayen, M. Xu, M. Zevallos, M. Alrubaiee, M. Lax, and R. R. Alfano, "Optical tomographic image reconstruction from ultrafast time-sliced transmission measurements," *Appl. Opt.*, vol. 38, no. 19, pp. 4237–4246, 1999.
[18] M. Xu, M. Alrubaiee, S. K. Gayen, and R. R. Alfano, "Three-dimensional localization and optical imaging of objects in turbid media using independent component analysis," *Appl. Opt.*, vol. 44, pp. 1889–1897, 2005.
[19] Z.-M. Wang, G. Y. Panasyuk, V. A. Markel, and J. C. Schotland, "Experimental demonstration of an analytic method for image reconstruction in optical diffusion tomography with large data sets," *Opt. Lett.*, vol. 30, pp. 3338–3340, Dec. 2005.
[20] M. Xu, M. Alrubaiee, S. K. Gayen, and R. R. Alfano, "Optical imaging of turbid media using independent component analysis: Theory and simulation," *J. Biomed. Opt.*, vol. 10, pp. 051705-1–051705-12, 2005.
[21] P. Comon, "Independent component analysis—A new concept?," *Signal Process.*, vol. 36, pp. 287–314, 1994.
[22] A. J. Bell, "Information theory, independent component analysis, and applications," in *Unsupervised Adaptive Filtering*, vol. I, S. Haykin, Ed. New York: Wiley, 2000, pp. 237–264.
[23] R. Vigário, J. Särelä, V. Jousmäki, M. Hämäläinen, and E. Oja, "Independent component approach to the analysis of EEG and MEG recordings," *IEEE Trans. Biomed. Eng.*, vol. 47, no. 5, pp. 589–593, May 2000.
[24] B. B. Biswal and J. L. Ulmer, "Blind source separation of multiple signal sources of f MRI data sets using independent component analysis," *J. Comput. Assist. Tomogr.*, vol. 23, no. 2, pp. 265–271, 1999.
[25] M. Alrubaiee, M. Xu, S. K. Gayen, and R. R. Alfano, "Tomographic imaging of scattering objects in tissue-like turbid media using independent component analysis," *Appl. Phys. Lett.*, vol. 87, pp. 191112-1–191112-3, 2005.
[26] M. Alrubaiee, M. Xu, S. K. Gayen, and R. R. Alfano, "Localization and cross-section reconstruction of fluorescent targets in *ex vivo* breast tissue using independent component analysis," *Appl. Phys. Lett.*, vol. 89, pp. 133902-1–133902-3, 2006.
[27] M. A. O'Leary, D. A. Boas, B. Chance, and A. G. Yodh, "Experimental images of heterogeneous turbid media by frequency-domain diffusing-photon tomography," *Opt. Lett.*, vol. 20, pp. 426–428, 1995.
[28] M. Xu, M. Lax, and R. R. Alfano, "Time-resolved Fourier optical diffuse tomography," *J. Opt. Soc. Amer. A*, vol. 18, no. 7, pp. 1535–1542, 2001.
[29] P. M. Morse and H. Feshbach, *Methods of Theoretical Physics*, vol. I/II. New York: McGraw-Hill, 1953.
[30] M. Alrubaiee, S. K. Gayen, R. Alfano, and J. A. Koutcher, "Spectral and temporal near-infrared imaging of *ex vivo* cancerous and normal human breast tissues," *Tech. Cancer Res. Treat.*, vol. 4, pp. 457–469, 2005.

**Min Xu** received the B.S. and M.S. degrees from Fudan University, Shangai, China, in 1992 and 1995, respectively, and the Ph.D. degree from the City University of New York, New York, in 2001, all in physics.

He is currently an Assistant Professor in the Department of Physics, Fairfield University, Connecticut. His recent work in biomedical optics has been on modeling light scattering by cells and human tissues, and developing optical spectroscopic and tomographic methods for cancer detection. He is the author or coauthor of more than 35 peer-reviewed papers published in various international journals and also the coauthor of the book *Random Processes in Physics and Finance* (Oxford University Press, 2006). His current research interests include wave scattering and propagation in random media and coherent phenomenon, radiative transfer of polarized light, random processes and Monte Carlo methods, biomedical optics, and inverse problems in applied physics and engineering.

**Mohammad Alrubaiee** received the B.Sc. degree in electric engineering and the M.Sc. degree in physics from the City College, City University of New York, in 1993 and 1999, respectively, and the Ph.D. degree in physics from the Graduate Center of the City University of New York, in 2007.

He is currently a Research Associate at the Institute for Ultrafast Spectroscopy and Laser, City College, City University of New York. His current research interests include time-resolved and optical spectroscopic imaging of biomedical media and optical tomography. He is the author or coauthor of more than 12 articles published in various refereed journals.

**S. K. Gayen** received the B.Sc. (Hons.) and M.Sc. degrees from the University of Dacca, Dacca, Bangladesh, in 1975 and 1977, respectively, and the Ph.D. from the University of Connecticut, Storrs, in 1984.

He is currently a Professor of physics at the City College and the Graduate Center of the City University of New York, New York. His current research interests include optical biomedical imaging, imaging of targets in turbid media, tunable solid-state lasers, spectroscopy of impurity ions in solids, nonlinear optics, ultrafast laser spectroscopy, and optical spectroscopy and microscopy of nanocomposites.

Dr. Gayen is a member of the American Physical Society and the Optical Society of America.

**R. R. Alfano** (M'87–SM'89–F'01) received the B.S. and M.S. degrees from Fairleigh Dickinson University, Hackensack, NJ, in 1963 and 1964, respectively, and the Ph.D. degree from New York University, in 1972, all in physics.

He is currently a Distinguished Professor of science and engineering at the City College and the Graduate Center of the City University of New York, New York. He is also the Director of the Institute for Ultrafast Spectroscopy and Lasers and the DoD Center for Nanoscale Photonic Emitters and Sensors at the City College. His current research interests include optical biomedical imaging, photon propagation through turbid media, ultrafast laser science and technology, ultrafast supercontinuum generation, tunable solid-state lasers, nonlinear optics, laser-induced shock waves, terahertz spectroscopy, as well as dynamical processes in semiconductors, dielectric crystals, molecular systems, polymers, and biological systems. He is the author or coauthor of more than 650 papers published in various international journals, edited four books and several conference proceedings, and organized several major conferences. He is the holder of 101 patents.

Dr. Alfano is a Fellow of the American Physical Society, IEEE and the Optical Society of America.